PLANT SPACING CONTROL FOR POTATO PLANTER BASED ON BP NEURAL NETWORK PID ALGORITHM

/

基于 BP 神经网络 PID 的马铃薯播种机株距控制研究

Xinlin LI[1)], Hongzhu WU[3)], Huan ZHANG*[1)], Zhiguo PAN[1)], Ranbing YANG[1,2)], Yue SHI[1)], Yihui MIAO[1)], Xuan LUO[1)], Zhaoming SU[1)], Shuai WANG[1)]

[1)]College of Mechanical and Electrical Engineering, Qingdao Agricultural University Qingdao /China

[2)]College of Mechanical and Electrical Engineering, Hainan University, Haikou /China

[3)]Qingdao Hongzhu Agricultural Machinery Co., Ltd., Qingdao /China

Tel: +86 13864215762; E-mail: huan0804@163.com

Corresponding author: Huan ZHANG

DOI: https://doi.org/10.35633/inmateh-78-09

Keywords: *electric-driven planter, velocity control, plant spacing control, neural network algorithm; co-simulation, field experiment*

ABSTRACT

To address the challenges of unstable planting spacing and susceptibility to operational fluctuations during the operation of electric-driven potato planters, an electric-driven spacing control system based on a BP neural network–PID controller was designed. The system uses actual output data from the rotational speed sensor, analog voltage signals from the control terminal, and control error information as inputs. By leveraging the online learning and adaptive tuning capabilities of the BP neural network, PID parameters are dynamically generated and optimized for real-time operating conditions, thereby achieving precise speed control of the seeding actuator. By integrating the structural design of the electric-driven potato planter with the spacing control mechanism, a mathematical model of the brushless DC motor and transmission system was established. Based on this model, a BP neural-network-based PID control strategy was developed. A MATLAB/Simulink simulation platform was constructed for comparative validation. Compared with a traditional PID controller tuned by empirical trial-and-error, the proposed method demonstrated superior control performance. The traditional PID exhibited approximately 10%–15% overshoot with oscillations during step response, whereas the neural network PID maintained a comparable rise time with negligible overshoot and a smoother response. Finally, both control algorithms were deployed on prototype machines for field trials to validate their effectiveness and engineering applicability under real-world conditions. Field test results indicated that under neural network control, the maximum row spacing error was 1.1 cm, with an average absolute relative error of 2.7%, meeting the row spacing accuracy requirements for electric-driven potato planters. These findings provide a theoretical basis and practical reference for the design of row spacing control systems in potato planters.

摘要

针对电驱马铃薯播种机作业过程中播种株距难以稳定、易受工况波动影响的问题，本文设计了一种基于 BP 神经网络 PID 的电驱株距控制系统。该系统以转速传感器反馈的实际输出、控制端模拟量电压以及控制误差等信息为输入，利用 BP 神经网络在线学习与自适应整定，实时给出更匹配工况的 PID 参数，从而实现对排种执行机构的精细调速控制。结合电驱马铃薯播种机的结构方案与株距控制机理，建立直流无刷电机及传动环节的数学模型，并在此基础上构建 BP 神经网络 PID 控制策略。进一步搭建 Matlab/Simulink 仿真平台开展对比验证：与采用经验试凑法整定的传统 PID 相比，所提方法控制性能更优：传统 PID 在阶跃响应中出现约 10%到 15%的超调并伴随一定振荡，而神经网络 PID 在基本保持上升速度的同时几乎无超调、响应更为平稳。最后，将两种控制算法分别部署于样机并开展田间试验，以进一步验证其在实际作业条件下的有效性与工程适用性。田间试验结果表明，神经网络控制下最大株距误差为 1.1cm，平均绝对相对误差为 2.7%，满足电驱马铃薯播种株距精度要求，研究成果可为马铃薯播种机株距控制系统提供理论依据与实践参考。

INTRODUCTION

China ranks among the world's largest producers and consumers of potatoes. Potatoes offer distinct advantages as a dual-purpose crop for both grain and vegetable production, with notable cold tolerance and

ability to thrive in poor soils. They play a vital role in safeguarding national food security and boosting farmers' incomes. Currently, China's potato planting area remains at a high level *(Guan et al., 2019)*, yet mechanization in the seeding process remains relatively low *(Lu et al., 2024).* Existing potato seeders predominantly use mechanically driven wheel-based seed distribution systems. Adjusting planting spacing requires manual sprocket replacement *(Singh et al., 2024)*, resulting in poor *portability*. Maintaining consistent spacing becomes challenging during frequent speed changes or turns. While a few potato planters employ electric-driven seed distribution, their control systems primarily rely on rudimentary throttle regulation. This approach suffers from low precision and insufficient automation/intelligence. During field operations, the control system struggles to rapidly adapt to changes in working speed; seeding speed adjustments are delayed, leading to spacing errors that disrupt field population structure and reduce seed potato utilization efficiency. This hinders achieving high and stable potato yields *(Xu et al., 2024)*.

In response to this challenge, numerous scholars have investigated plant-spacing control strategies for a range of crops. *Liu et al. (2023)* developed an adjustable in-row spacing grape seedling transplanter in which the target plant spacing can be set as a function of forward travel speed. *Siemens et al. (2016)* compared vacuum and belt planters for precision lettuce seeding across travel speeds, evaluating spacing uniformity and closely spaced seeds. *Chen et al. (2022)* analyzed the key factors influencing seed placement and proposed a fuzzy PID–based dynamic compensation system for corn seeding position. *Zhang et al. (2023)* developed a compact pneumatic precision vegetable seeder for protected greenhouse production; by replacing the seed plate and divider, the machine can perform single-, double-, or triple-row seeding. *Karayel et al. (2008)* evaluated three depth-control components with different furrow openers and quantified effects on in-row spacing uniformity and seed placement using mean, standard deviation, and coefficient of variation. They showed these configurations affect spacing consistency and emergence. *Yao et al. (2022)* investigated a vacuum-disc corn metering device and designed a fuzzy PID–controlled unit drive for a precision corn planter, achieving high positioning accuracy. *Sharaby et al. (2019)* compared representative precision seed planters worldwide in terms of metering and delivery mechanisms, operating requirements, and their ability to regulate seeding rate and in-row spacing. *Zubrilina et al. (2019)* proposed a precision seeding planter with automated monitoring and control to coordinate seed motion with forward speed. *Chen et al. (2022)* designed an electrically driven precision seeding control system based on an STM32 microcontroller and CANopen; operating speed was obtained via GPS, and after the target plant spacing was specified, a PID controller was used to match the metering mechanism speed to the travel speed.

To enhance the stability and dynamic tracking capability of the seeding system for electric-driven potato planters, this paper designs a row spacing control system for electric-driven potato planters based on a neural network PID algorithm. Grounded in PID control theory and incorporating neural network algorithms, the system establishes a mathematical model of the control object and conducts MATLAB/Simulink simulation experiments. Performance metrics—including overshoot, rise time, and steady-state time of the system response curve—are compared with those of classical PID control. Field trials validate the system's practical control performance relative to traditional PID control, providing theoretical justification and empirical data for improving row spacing control systems in electric-driven seeders.

MATERIALS AND METHODS

Potato Electric-Powered Planter Overall Structure

The overall structural design of the potato electric-powered seeder is shown in Figure 1.

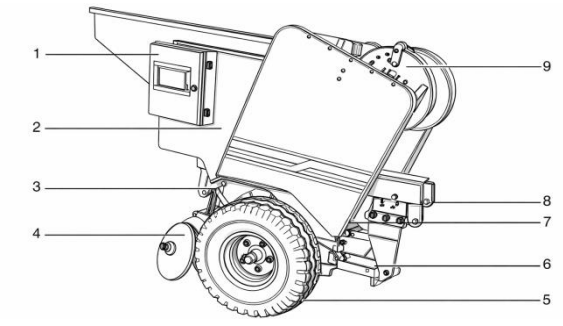

Fig. 1 – Schematic diagram of the electric-driven seeder assembly

1 - Electrical Control Panel; 2 - Seedling tray; 3 - Optical rotary encoder; 4 - Covering disc; 5 - Ground wheel; 6 - Ditch digger; 7 - Brushless DC motor; 8 - Gearbox; 9 - Seeding system

The electric-driven potato planter is a rear-mounted, dual-furrow, dual-row tractor-mounted seeder. The main components include the frame and mounting assembly, seed hopper and seed delivery mechanism, electric-driven seed metering device, furrow-opening and soil-covering unit, travel and depth-limiting mechanism, and electrical control system. The frame employs a welded box-type structure connected to the tractor's three-point hitch. The upper section houses a large-capacity compartmentalized seed hopper, featuring an inclined flow-limiting plate and grid at the bottom to ensure uniform seed delivery. Each row in the middle section is equipped with a chain-scoop seed dispenser driven by a brushless DC motor via a coupling. The motor speed is continuously adjustable through control signals received by the drive unit, dispensing seed potatoes into the seed furrows. The front-lower furrow opener digs seed furrows, while a rear pair of soil-covering discs completes soil backfilling and ridge compaction. The electrical and control system comprises motor drivers, power supplies, and speed detection units *(Lyu et al., 2018)*. It enables real-time control of seed dispensing shaft speed based on ground wheel encoder or tractor speed signals, achieving precise plant spacing control. A reserved human-machine interface module facilitates future expansion for operational status monitoring and intelligent regulation functions.

Principle of the Potato Electric-Driven Planter Row Spacing Control System

The row spacing control system for the electric-driven seeder primarily consists of a speed detection unit, a gear transmission system, a SIEMENS S7-200 series PLC, a brushless DC motor, and its corresponding driver. During field operations, the electric-driven seeder is towed forward by a tractor and rigidly connected to the tractor via a three-point hitch. A rotary encoder is fixed to the wheel axle of the seeder's ground wheel, continuously capturing ground wheel rotation speed and converting it into forward speed signals input to the Siemens S7-200 PLC. Internally, the PLC calculates the desired motor speed based on the target plant spacing and measured forward speed, executes control algorithms, and outputs an analog voltage signal. The brushless DC motor driver receives this voltage signal to drive the brushless DC motor to achieve the corresponding rotational speed. The motor output is reduced through a fixed-ratio gearbox to drive the seeder's drive shaft. This shaft then drives the seed belt's driven shaft via gear transmission, matching the seed unit's rotational speed to the machine's forward speed *(Gui et al., 2024; Zhu et al., 2021)*. This achieves precise row spacing control through the “ground wheel encoder – PLC control – motor drive – mechanical transmission” system, as illustrated in Figure 2.

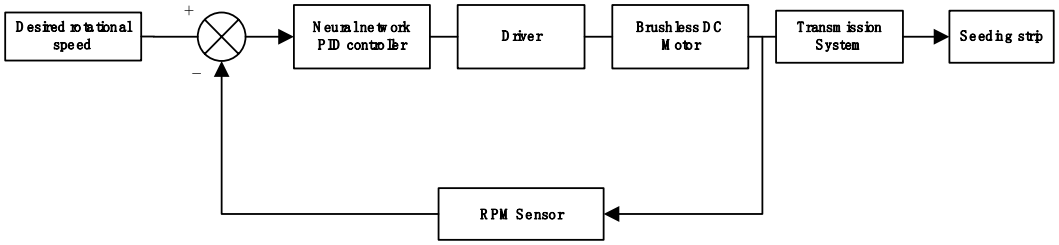

Fig. 2 – Plant Spacing Control System Schematic Diagram

The seeding mechanism of the planter is illustrated in Figure 3.

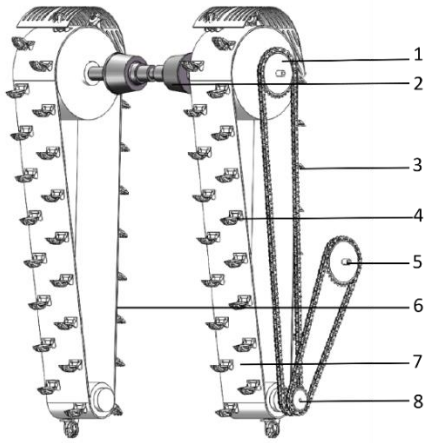

Fig. 3 – Schematic diagram of seed placement system operation

1 - Sprocket 1; 2 - Synchronous shaft; 3 - Chain; 4 - Seed scoop;
5 - Sprocket 2; 6 - Seeding area; 7 - Seed strip; 8 - Sprocket 3

Upon receiving control voltage signals, the brushless DC motor generates torque. This torque is transmitted through a reduction gearbox, which lowers speed while increasing torque, converting the motor's high-speed rotation into the low-speed rotation of sprocket *2*. Acting as the drive sprocket, sprocket *2* drives sprocket *3* and sprocket *4* in sequence via the chain drive, synchronizing their rotation and thereby propelling the seed delivery belt into continuous operation. When the seed scoop reaches the highest point along the seed distribution belt and enters the seeding zone, its orientation inverts. The scoop tilts downward, allowing seed potatoes to dislodge from the scoop under gravity and fall into the seed outlet, ultimately completing placement into the furrow.

Mathematical Model of the Control Object

This design controls a three-phase brushless DC motor with symmetrical parameters. Under conditions in which nonlinear factors such as magnetic saturation, cogging torque, and viscous damping are neglected, the three-phase brushless DC motor can be equivalently modeled as a single-input single-output average model, as shown in Figure 4.

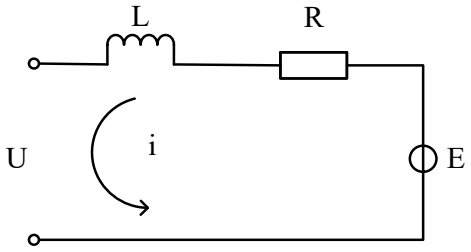

Fig. 4 – Equivalent average model

The voltage, electromagnetic torque, and mechanical motion equations of the brushless DC motor was described by the following Equations (1-3):

$$U = L\frac{di}{dt} + Ri + k_d\omega \tag{1}$$

$$T_e = k_m i \tag{2}$$

$$J\frac{d\omega}{dt} + M_L = T_e \tag{3}$$

Simplifying Equations (1-3) yields Equation (4):

$$i = \frac{J}{k_m}\frac{d\omega}{dt} + \frac{1}{k_m}M_L \tag{4}$$

Differentiation yields Equation (5):

$$\frac{di}{dt} = \frac{J}{k_m}\frac{d^2\omega}{dt^2} + \frac{1}{k_m}\frac{dM_L}{dt} \tag{5}$$

Substituting Equations (4-5) into the voltage Equation (1) yields Equation (6):

$$\frac{LJ}{k_d k_m}\frac{d^2\omega}{dt^2} + \frac{RJ}{k_d k_m}\frac{d\omega}{dt} + \omega = \frac{1}{k_d}U - \frac{L}{k_d k_m}\frac{dM_L}{dt} - \frac{R}{k_d k_m}M_L \tag{6}$$

Applying the Laplace transform to equation (6) and setting the initial conditions to zero yields the motor angular velocity:

$$\Omega(s) = \frac{\frac{1}{k_d}U(s) - \left(\frac{L}{k_d k_m}s + \frac{R}{k_d k_m}\right)M_L(s)}{\frac{LJ}{k_d k_m}s^2 + \frac{RJ}{k_d k_m}s + 1} \tag{7}$$

Neglecting load torque disturbances and setting $M_L(s)=0$ yields the transfer function from motor output voltage to output angular velocity as:

$$G(s) = \frac{\Omega(s)}{U(s)} = \frac{\frac{1}{k_d}}{\frac{LJ}{k_d k_m}s^2 + \frac{RJ}{k_d k_m}s + 1} \tag{8}$$

where:

U – armature voltage applied to the equivalent circuit, V;

i – armature current applied to the equivalent circuit, A;

R – equivalent resistance, Ω;

L – equivalent inductance, H;

Ω – output angular velocity of the motor, rad/s;
k_d – reverse voltage constant, V·s/rad;
k_m – current-torque constant, N·m/A;
J – moment of inertia, kg·m²;
M_L – Load torque, N·m;
T_e – Electromagnetic torque, N·m.

Design of BP Neural-network-based PID controller

PID controller

PID control holds significant engineering value in brushless motor speed regulation and servo control applications. By appropriately adjusting control parameters, it can partially compensate for system nonlinearities, thereby enhancing control performance and stability. The fundamental architecture of a PID control system comprises three core components: the controller module, the actuator, and the feedback detection unit, as illustrated in Figure 5. The controller module performs algorithmic computations, the actuator implements control outputs, and the feedback detection unit enables real-time monitoring and feedback of the system's state *(Lyu et al., 2021)*.

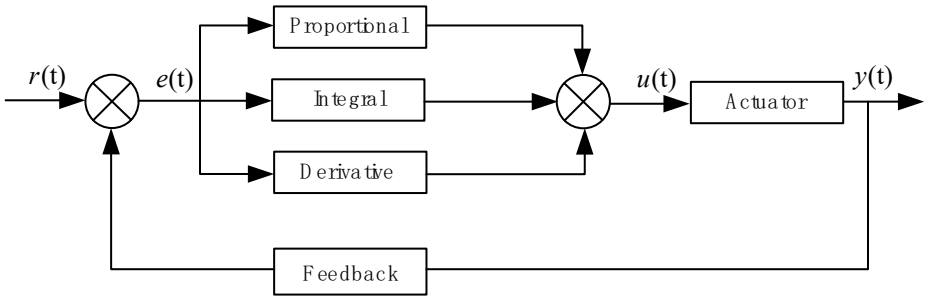

Fig. 5 – PID control system schematic diagram

Based on the schematic diagram, the system deviation *e(t)* is as follows:

$$e(t) = r(t) - y(t) \tag{9}$$

The PID controller adjusts control parameters online based on the system error e(t), thereby generating the control output u(t) to the target system yields Equation (10):

$$u(t) = K_p e(t) + K_i \int_0^t e(\tau)\, d\tau + K_d \frac{de(t)}{dt} \tag{10}$$

By applying discretization and weighting to the integral term, the incremental PID formula is obtained as shown in Equation (11):

$$\Delta u(k) = K_p(e(k) - e(k-1)) + K_i e(k) + K_d(e(k) - 2e(k-1) + e(k-2)) \tag{11}$$

where:

$r(t)$ is the system input;
$y(t)$ – system output;
$u(t)$ – controller output;
K_p – proportionality coefficient;
K_i – integral coefficient;
K_d – derivative coefficient.

Neural-network-based PID controller

Traditional PID control features a simple structure and mature engineering implementation, delivering good dynamic and steady-state performance under conditions where the controlled object is approximately linear and parameters remain relatively constant. However, the row spacing control system of potato planters is significantly affected by factors such as ground undulations, tire slippage, load fluctuations, and transmission backlash during field operations. The system's equivalent parameters exhibit time-varying and nonlinear characteristics as they change with speed and operating conditions. Against this backdrop, traditional PID controllers with fixed parameters often deliver optimal performance only near specific operating conditions. When working speed or external disturbances change, control quality deteriorates, manifesting as degraded tracking performance, increased risk of overshoot and oscillation, and amplified steady-state error. Even

parameters obtained through repeated offline tuning struggle to simultaneously satisfy the requirements for rapid response, stability, and disturbance rejection across different operational phases.

To overcome the limited adaptability to operating conditions caused by fixed traditional PID parameters, a neural-network-based PID control strategy is introduced. BP neural networks have been applied in agricultural machinery multisensor fusion and control, as well as precision agriculture decision-making (fertilization and irrigation) *(Ji et al., 2023; Xia et al., 2015; Dong et al., 2020)*. The core concept involves utilizing a neural network to learn the nonlinear mapping relationship between system operating conditions and control performance. During operation, PID parameters are dynamically adjusted based on real-time error feedback and changing operating conditions. This enables the controller gains to adaptively vary with system state, generating an appropriate analog voltage signal $u(k)$to control the speed of the brushless DC motor, thereby adjusting the seeding spacing.

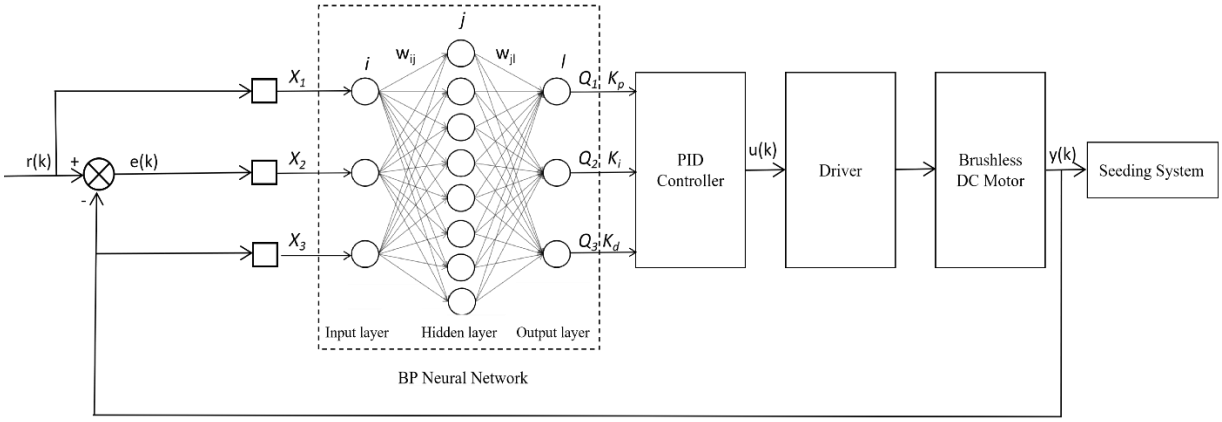

Fig. 6 – Neural-network-based PID controller architecture

In this paper, the BP neural network adopts a three-layer (3-8-3) structure, comprising 3 input layer nodes, 8 hidden layer nodes, and 3 output layer nodes. The neural network inputs include the desired system output speed *r(k)*, the actual value *y(k)*, and the output error *e(k)*, as illustrated in Figure 6.

The output of the input layer of the BP neural network is:

$$Q_i = x(i),\ i = 1,2,3 \tag{12}$$

The input and output of the hidden layer are given by Equations (13-14):

$$Nj(k) = \sum_{i=1}^{3} \omega_{ij} Q_i\,(k) \tag{13}$$

$$Q_j(k) = f\left(N_j(k)\right), j = 1,2,3,\ldots 8 \tag{14}$$

f(x) is the hidden layer activation function, which employs a bipolar sigmoid function. The sigmoid function was the preferred activation function in early neural networks. By stacking neurons with sigmoid activation, the network can approximate any continuous function. It possesses certain biomimetic properties, approximating the response patterns of biological neurons by simulating the "activation-inhibition" characteristics of neurons. The *f(x)* function is defined as:

$$f(x) = \frac{1}{1+e^{-x}} \tag{15}$$

The input and output of the output layer are given by Equations (16-17).

$$N_l(k) = \sum_{j=1}^{8} \omega_{jl} Q_j(k) \tag{16}$$

$$Q_l(k) = g\left(N_l(k)\right),\ l = 1,2,3 \tag{17}$$

The output of the output layer and the output of the backpropagation neural network correspond to the optimized PID parameters, namely $Q_1=K_p$, $Q_2=K_i$, $Q_3=K_d$. In the equation, *g(x)* represents the output layer activation function, which employs a unipolar sigmoid function. While sigmoid functions may exhibit vanishing gradients when inputs are extremely large or small, they maintain good numerical stability when applied to the output layer. The *g(x)* function is defined as:

$$g(x) = \frac{1}{2}(1 + tahn(x)) = \frac{e^x}{e^x+e^{-x}} \tag{18}$$

Adjust the weighting coefficients to reduce the angular velocity error of the motor output, and take the neural network performance indicator function *E(k)*:

$$E(k) = \frac{1}{2}(r(k) - y(k))^2 = \frac{1}{2}e^2(k) \quad (19)$$

The gradient descent method is employed to adjust the weight coefficients of each layer in the neural network. Weights are modified along the negative gradient direction of the error function to progressively reduce the loss. The weight update amount $\Delta\omega jl(k)$ from the hidden layer to the output layer is given by Equation (20):

$$\Delta\omega_{jl}(k) = -\eta\frac{\partial E(k)}{\partial\omega_{jl}} + \alpha\Delta\omega_{jl}(k-1) \quad (20)$$

Taking the partial derivative with respect to ω_{jl}, the chain expansion for $\frac{\partial E(k)}{\partial\omega_{jl}}$ is given by Equation (21):

$$\frac{\partial E(k)}{\partial\omega_{jl}(k)} = \frac{\partial E(k)}{\partial e(k)}\frac{\partial e(k)}{\partial y(k)}\frac{\partial y(k)}{\partial u(k)}\frac{\partial u(k)}{\partial Q_l(k)}\frac{\partial Q_l(k)}{\partial N_l(k)}\frac{\partial N_l(k)}{\partial\omega_{jl}(k)} \quad (21)$$

$$\text{Defined } \frac{\partial y(k)}{\partial u(k)} = sat\left(\frac{y(k)-y(k-1)}{u(k)-u(k-1)}\right) \quad (22)$$

From Equations (20–22), Equation (23) is obtained:

$$\frac{\partial E(k)}{\partial\omega_{jl}(k)} = -e(k)\,sat\left(\frac{y(k)-y(k-1)}{u(k)-u(k-1)}\right)\frac{\partial u(k)}{\partial Q_l(k)}g'(N_l(k))Q_j(k) \quad (23)$$

The output error signal is defined as in Equation (24):

$$\delta_l(k) = -e(k)\,sat\left(\frac{y(k)-y(k-1)}{u(k)-u(k-1)}\right)\frac{\partial u(k)}{\partial Q_l(k)}g'(N_l(k)) \quad (24)$$

From equations (20–24), Equation (25) is obtained:

$$\Delta\omega_{jl}(k) = \eta\delta_l(k)Q_j(k) + \alpha\Delta\omega_{jl}(k-1) \quad (25)$$

Similarly, the weight update *Δωij(k)* from the input layer to the hidden layer is given by Equation (26):

$$\Delta\omega_{ij}(k) = \eta\delta_l(k)Q_i(k) + \alpha\Delta\omega_{ij}(k-1) \quad (26)$$

where: *r(k)* – desired output angular velocity, rad/s;

y(k) – actual output angular velocity, rad/s;

sat(x) – symmetrical clipping function with an amplitude of 1;

η – neural network learning rate;

α– neural network inertia factor.

As shown by the above formula, neural network weight adjustment employs a momentum-based gradient descent approach, in which the update consists of both the current gradient term and the historical increment term. The learning rate η determines the step size of the weight along the negative gradient direction, thereby influencing the convergence speed and stability of the network's output parameters. Combined with the momentum factor α and the weight increment from the previous moment, it suppresses oscillation, smooths updates, and accelerates convergence. Considering the practical requirements of the row spacing control system, the learning rate η is set to 0.1 and the momentum factor α to 0.85.

Simulink Modeling and MATLAB Simulation

The mathematical model of the DC brushless motor under control in this design is given by Equation (27):

$$G(s) = \frac{4.065}{0.00016s^2 + 0.057s + 1} \quad (27)$$

Based on PID control principles, the system was simulated using the Simulink simulation tool in MATLAB software. The neural network's hidden layer was constructed using the function block. The simulation model is shown in the Figure 7. To validate the effectiveness and superiority of the BP neural-network-based PID control strategy on the control object discussed in this paper, both a BP neural-network-based PID control simulation model and a traditional PID control simulation model with parameters tuned using the empirical trial-and-error method were established. The output responses of both models were compared, as illustrated in Figure 8.

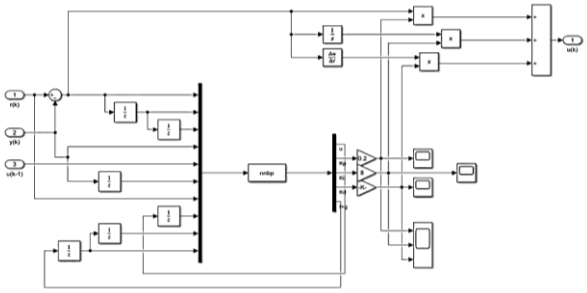

Fig. 7 – BP neural network simulation model

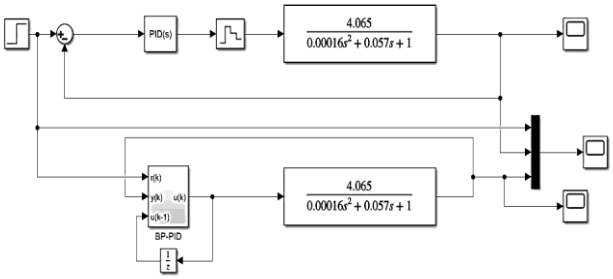

Fig. 8 – BP Neural Network PID vs. Traditional PID Comparison Model

RESULTS

Simulation results

Through trial-and-error methods, PID parameters were selected for the control object in this paper. The obtained PID parameters are Kp=30, Ki=0.1, Kd=1, serving as the traditional PID control parameter values. A step input with an amplitude of one was applied. The simulation time was set to 10 seconds, and the sampling period was set to 0.01 seconds. The response curves comparing the BP neural network PID and traditional PID are shown in Figure 9.

In actual field seeding operations, complex seeding conditions may cause imbalances in the plant spacing control system's performance. To validate the disturbance rejection capability of the BP neural-network-based PID control method, a transient disturbance signal was introduced at the 6-second mark of the simulation and rapidly withdrawn once the system stabilized. The resulting changes in response curves under both control methods are compared, as shown in Figure 10.

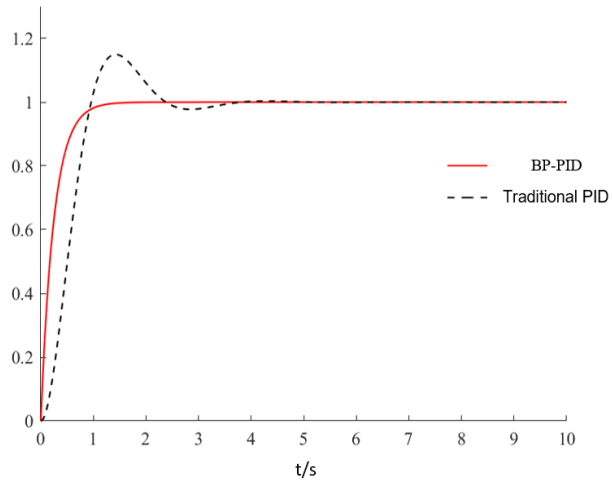

Fig. 9 – Comparison response curve

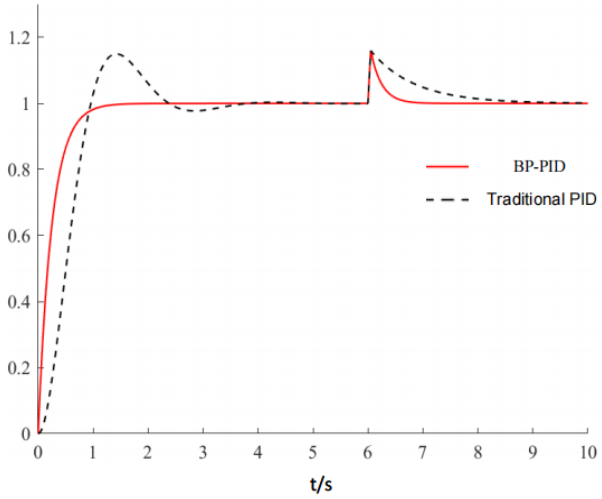

Fig. 10 – Contrast response curve under disturbance

Table 1

Comparison of Response Curve Data

Control method	Steady-state time/s	Steady-state error	Overshoot
BP-PID	1.76	0.009	0
Traditional PID	3.80	0.015	0.172

Calculations based on the data in Figure 9 and Table 1 indicate that under BP neural-network-based PID control, the system's steady-state error is reduced by 40% compared to traditional PID control, the steady-state time is shortened by 53.68%, and there is no overshoot.

As shown in Figure 10, the response curve of the traditional PID control method stabilizes at 3.20 seconds after disturbance withdrawal, while the BP neural-network-based PID control method achieves stabilization at 0.93 seconds after disturbance withdrawal. This represents a reduction of approximately 70.94% in response time. Therefore, the BP neural-network-based PID control method not only demonstrates significantly superior control performance compared to traditional PID but also exhibits certain advantages in disturbance rejection.

Field trial

To validate the effectiveness of the simulation-verified neural network PID algorithm in actual field seeding operations, a field trial was conducted on November 5, 2025, at the experimental field of Hongzhu Agricultural Machinery Co., Ltd. in Jiaolai Subdistrict, Jiaozhou City, Shandong Province. The trial hardware included an LPD3806-600BM-G5 rotary encoder, Siemens S7-200 PLC, 110BL168S150-430TKA brushless DC motor, MSSD-40SMA DC brushless driver, F700A touchscreen, RPM sensor, 24V switching power supply, 48V switching power supply, and high-precision multimeter. The seeder was towed by an Dongfenghong LX-604 tractor, with its power take-off unit connected to the generator set to supply electricity to all components.

Fig. 11 –Field trial process

To compare the row spacing control capability and stability of an electric-powered potato planter under two control methods during field operations, performance tests were conducted. The seeder's operating speed was set at 6 km/h. Six test groups were established based on row spacings of 22 cm, 25 cm, 27 cm, 30 cm, 32 cm, and 35 cm. Fifty seed potato sets were planted in each group. The spacing between adjacent seed potatoes was measured and recorded throughout the entire process. The average spacing was calculated for each group, and the spacing error and relative error were subsequently determined.

$$L = \frac{1}{n}\sum_{i=1}^{n} L_i \quad (28)$$

$$E_a = L - L_0 \quad (29)$$

$$E_r = \frac{E_a}{L_0} \times 100\% \quad (30)$$

where:

L – average plant spacing, cm;

L_i – actual plant spacing, i=1, 2, …, 50;

E_a – plant spacing error, cm;

L_0 – target plant spacing, cm;

E_r – relative error.

The experiment employed a Siemens S7-200 PLC as the controller. Programs corresponding to the two control strategies were downloaded to the PLC, and the aforementioned tests were conducted under identical experimental conditions. The results were then subjected to comparative analysis. The experimental results are presented in Table 2.

Table 2

Test result data

Test number	Target plant spacing	Traditional PID control			Neural-network-based PID control		
		Average plant spacing	Plant spacing error	Relative error	Average plant spacing	Plant spacing error	Relative error
1	22	23.7	+1.7	+7.7%	22.6	+0.6	+2.7%
2	25	26.2	+1.2	+4.8%	25.6	+0.6	+2.4%
3	27	25.6	-1.4	-5.2%	27.9	+0.9	+3.3%
4	30	30.9	+0.9	+3.0%	28.9	-1.1	-3.7%
5	32	34.2	+2.2	+6.9%	32.3	+0.3	+0.9%
6	35	33.4	-1.6	-4.6%	36.0	+1.0	+2.9%

As shown in Table 2, both traditional PID control with parameters obtained through empirical trial-and-error and neural-network-based PID control achieved planting row spacing close to the target spacing. Under traditional PID control, the maximum spacing error was 2.2 cm with an average absolute relative error of 5.4%. Under neural network control, the maximum spacing error was 1.1 cm with an average absolute relative error of 2.7%. The experimental results demonstrate that neural-network-based PID control exhibits superior precision in seed spacing regulation compared to traditional PID control, indicating certain advantages.

CONCLUSIONS

This study targets the demand for stable plant spacing control in field operation of an electric-driven potato planter. The work covers the structural design of the plant spacing control system, the development of a BP-neural-network-based PID control strategy, and validation via simulation and field experiments. By establishing a mathematical model of the electric drive transmission chain and a control-system simulation platform, the relationship between control parameters and planting spacing quality was clarified.

(1) An electric plant spacing control system was developed, consisting of a ground-wheel encoder, a PLC controller, a brushless DC motor, and a mechanical transmission chain. A mathematical model and transfer function of the controlled plant—the brushless DC motor—were derived, and the influence mechanisms of operating speed, transmission ratio, and motor speed-regulation characteristics on plant spacing uniformity were elucidated.

(2) A BP-neural-network PID control strategy with a 3-input, 8-hidden-neuron, and 3-output architecture was proposed. MATLAB programming and Simulink modeling were used to conduct comparative simulations against a conventional PID controller. The results show that, relative to conventional PID, the proposed controller reduces steady-state error by 40% and shortens settling time by 53.68%, while achieving zero overshoot. Under disturbance conditions, the recovery time is reduced by 70.94%, indicating improved stability and dynamic tracking performance.

(3) Comparative field experiments were performed for the BP-neural-network PID strategy and the conventional PID controller. Under conventional PID control, the maximum plant spacing error was 2.2 cm and the mean absolute relative error was 5.4%. Under BP-neural-network PID control, the maximum plant spacing error decreased to 1.1 cm and the mean absolute relative error to 2.7%. These results demonstrate that the proposed BP-neural-network PID controller provides higher plant-spacing precision than conventional PID control, and the overall operating quality meets the relevant agronomic requirements and applicable standards.

ACKNOWLEDGEMENT

This research was funded by the National Key R&D Program of China (Project no.2023YFD2000902).

REFERENCES

[1] Chen J., Zhang H., Pan F. (2022). Control system of a motor-driven precision no-tillage maize planter based on the CANopen protocol. *Agriculture*, 12(7), 932.

[2] Chen K., Yuan Y., Zhao B. (2022). Design of dynamic compensation system for corn seeding position based on fuzzy PID control and analysis of bench test. *INMATEH - Agricultural Engineering*, 67(2), 394–405.

[3] Dong Y., Fu Z., Peng Y. (2020). Precision fertilization method of field crops based on the Wavelet-BP neural network in China. *Journal of Cleaner Production*, 246, 118735.
[4] Guan J., Cai H. (2019). The characteristics and causes of changes in China's potato production pattern (我国马铃薯生产格局变化特征及原因分析). *China Agricultural Resources and Zoning*, 40(3), 92–100.
[5] Gui Z., Gu Y., Xu L. (2024). Design and testing of an electronic control system for wheat seeders based on GNSS speed measurement (基于 GNSS 测速的小麦播种机电控系统设计与试验). *Henan Agricultural University*, 30–37.
[6] Ji K., Li Y., Zhang T. (2023). Technology of adjusting the header height of the harvester by multi-sensor data fusion based on BP neural network. *INMATEH - Agricultural Engineering*, 68(3), 91–96.
[7] Karayel D., Özmerzi A. (2008). Evaluation of Three Depth-Control Components on Seed Placement Accuracy and Emergence for a Precision Planter. *Applied Engineering in Agriculture*, 24(3), 271–276.
[8] Liu F., Xu L., Niu C. (2023). Design and testing of an adjustable-row-Spacing grapevine transplant (株距可调式葡萄苗木栽植机设计与试验). *Journal of China Agricultural University*, 28(10), 184–193.
[9] Lu J., Liu S., Wang Q., Liao M. (2024). Research on device and sensing technology for precision seeding of potato. *Agriculture*, 14(12), 2146.
[10] Lyu H., Hu Z., Yu Y., Kang F. (2021). Feedforward PID control method for the automatic leveling of an orchard high-position operation platform (果园高位作业平台自动调平前馈 PID 控制方法). *Transactions of the Chinese Society of Agricultural Engineering*, 37(18), 20–28.
[11] Lyu J., Yi S., Tao G., Mao X. (2018). Parameter optimization and experiment of splitter sliding-knife opener for potato planter (马铃薯播种机分体式滑刀开沟器参数优化与试验). *Transactions of the Chinese Society of Agricultural Engineering*, 34(4), 44–54.
[12] Sharaby N., Doroshenko A., Butovchenko A. (2019). A comparative analysis of precision seed planters. *E3S Web of Conferences*, 135, 01080.
[13] Siemens M.C., Gayler R.R. (2016). Improving seed spacing uniformity of precision vegetable planters. *Applied Engineering in Agriculture*, 32(5), 579–587.
[14] Singh R.D. (2004). Tractor mounted semi-automatic two-row belt type potato planter ridger. *Agricultural Engineering Today*, 28, 69–74.
[15] Xia S., Zhao L. (2015). Multisensor information fusion study of basic BP neural network (基于 BP 神经网络的多传感器信息融合研究). *Computer measurement and Control*, 23(5), 1823–1826. Beijing/China.
[16] Xu T., Hao Z., Zhang Y., Xu K. (2024). Comparative experimental study on operation performance and yield of maize seeders of different types in wheat stubble. *INMATEH - Agricultural Engineering*, 74(3), 422–424.
[17] Yao Y., Chen X., Ji C., Zhang J. (2022). Design and experiments of the single driver for maize precision seeders based on fuzzy PID control (基于模糊 PID 控制的玉米精量播种机单体驱动器设计与试验). *Transactions of the Chinese Society of Agricultural Engineering*, 38(6), 12–21.
[18] Zhang Y., Yang X., Li X., Wang Z. (2023). Design and experiment of small vegetable seeder with single disc multi-row seeding and independent airway. *INMATEH - Agricultural Engineering*, 70(2), 37–45.
[19] Zhu W. (2021). Electric control system of picking manipulator based on PLC and PSO (基于 PLC 和粒子群算法的采摘机械手电气控制系统). *Journal of Agricultural Mechanization Research*, 43(12), 238–241, 246.
[20] Zubrilina E., Markvo I., Novikov V., Beskopylny A., Vysochkina L. (2019). Precise seeding planter with automated monitoring and control system. *IOP Conference Series: Earth and Environmental Science*, 403, 012063.